DOI: 10.1002/ ((please add manuscript number))

Article Type: Full Paper

Random Copolymers Outperform Gradient and Block Copolymers in Stabilizing Organic Photovoltaics.

*Chen Kong,† Byeongseop Song,† Emily A. Mueller, Jinsang Kim and Anne J. McNeil**

Dr. Chen Kong, Emily A. Mueller, Prof. Anne J. McNeil

Department of Chemistry and Macromolecular Science and Engineering Program, University of Michigan, 930 North University Avenue, Ann Arbor, Michigan 48109-1055, United States

Email: ajmcneil@umich.edu

Dr. Byeongseop Song

Department of Electrical Engineering and Computer Science, University of Michigan

Prof. Jinsang Kim

Departments of Materials Science and Engineering, Macromolecular Science and Engineering, Chemistry, Chemical Engineering, University of Michigan

†These authors contributed equally.

Keywords: conjugated polymers, fullerenes, polymer blends, organic photovoltaics

Abstract

Recent advances have led to conjugated polymer-based photovoltaic devices with efficiencies rivaling amorphous silicon. Nevertheless, these devices become less efficient over time due to changes in active layer morphology, thereby hindering their commercialization. Copolymer additives are a promising approach towards stabilizing blend morphologies, however, little is known about the impact of copolymer sequence, composition, and concentration. Herein, we determine the impact of these parameters by synthesizing random, block, and gradient copolymers with a poly(3-hexylthiophene) (P3HT) backbone and side-chain fullerenes ($PC_{61}BM$). We evaluate these copolymers as compatibilizers in photovoltaic devices with P3HT:$PC_{61}BM$ as the active layer. The random copolymer with 20 mol% fullerene side chains and at 8 wt% concentration in the blend gave the most stable morphologies. Devices containing the random copolymer also exhibited higher and more stable power conversion efficiencies than the control device. Combined, these studies point to the random copolymer as a promising new scaffold for stabilizing bulk heterojunction photovoltaics.

1. Introduction

The National Renewable Energy Lab (NREL) has been tracking the "best" photovoltaic cells since 1976, highlighting growth trends in promising materials and technologies.[1] Conjugated polymer-based solar cells exhibit some of the lowest efficiencies on this chart, but are considered 'emerging' materials because of their advantageous properties, including transparency, flexibility, and low weight.[2] In addition, the solution-based processing methods used for device fabrication is commercially appealing.[3] As a consequence, many researchers continue searching for organic materials with higher efficiencies.

Most organic photovoltaics are constructed from a blend of two materials: a conjugated polymer electron donor and a small molecule electron acceptor. The optoelectronic properties and device performance are dictated by the chemical structures of both components as well as the blend morphology. Recent advances in both donor and acceptor structures have led to organic devices with efficiencies that rival amorphous silicon.[4,5] As an example, Hou and co-workers described a novel blend with a record-breaking 14.2% efficiency.[4b] This device has not

yet been certified by NREL due to its instability. In a corresponding highlight article, Hou suggests that conjugated polymer-based devices may reach 18–20% efficiency within the next few years.[6]

With efficiencies on the rise, many researchers are focused on improving device longevity. Due to changes in the active layer morphology, organic photovoltaic devices gradually lose efficiency over time.[7] The initial active layer morphology consists of nanoscale phase-separated P3HT and $PC_{61}BM$ domains. These domains coalesce, increasing in size over time due to enthalpically-driven phase separation.[8] The net result is that the power conversion efficiencies (PCE) dramatically decrease, reducing the device utility.

To attenuate this detrimental process, researchers are investigating compatibilizers – a third component added to the blend to stabilize the morphology through non-covalent interactions.[9] To be effective, the compatibilizer should minimize the overall free energy by localizing at the donor/acceptor interface, lowering the interfacial tension and suppressing domain coalescence. The compatibilizer can impart additional beneficial properties to the device, such as a broader and stronger absorption profile as well as more efficient exciton dissociation and charge transport, all of which would contribute to a higher PCE.[9]

Both small molecules[10] and polymers[11,12] have been used as compatibilizers with moderate success. The majority of polymer compatibilizers have been diblock copolymers containing repeat units that are structurally similar to the donor and acceptor.[12] A prototypical example is a rod–coil diblock copolymer with a conjugated segment (the rod) that resembles the donor polymer and a nonconjugated segment (the coil) with a side-chain group that interacts with the acceptor. One limitation of this approach is that the coil segment is frequently an

insulating material, which lowers the effective concentration of absorbing and electroactive species in the device. Rod–rod diblock copolymers wherein both segments are conjugated have also been used.[12] These copolymers can facilitate exciton dissociation and charge transport as well. Although adding these tailored compatibilizers provides longer-lasting devices, no studies have elucidated the impact of sequence (e.g., block versus gradient) or composition (e.g., 50:50 versus 25:75) on compatibilization.

To address this knowledge gap, we have been exploring alternative copolymer sequences (i.e., random[13] and gradient[14,15] copolymers) as compatibilizers in blends. For example, we reported that gradient copolymer compatibilizers led to smaller domain sizes than the analogous block and random copolymers in homopolymer blends.[14] Gradient copolymers, with their gradual compositional change, were best at interacting with both homopolymer domains to lower the interfacial energy. In related work, we found that a gradient copolymer could stabilize photovoltaic devices containing poly(3-hexylthiophene) (P3HT) and phenyl-C_{61}-butyric acid methyl ester ($PC_{61}BM$), with little change in efficiency over extended thermal annealing times (> 60 min at 150 °C).[15]

Herein, we expand on this work by examining the influence of copolymer sequence (random, diblock, and gradient), composition (co-monomer ratio), and concentration on the stabilization of P3HT:$PC_{61}BM$ blends. All copolymers attenuated phase separation during thermal annealing. Their compatibilizing abilities depended on copolymer sequence, with gradient and random sequences outperforming the analogous diblock sequences. Further studies showed that the random copolymer gave a higher and longer-lasting PCE than the blend without copolymer. These improvements were due to the random copolymer's ability to stabilize the morphology, as well as facilitate exciton dissociation and charge transport.

Combined, these results suggest that random copolymers are the best compatibilizers for stabilizing organic photovoltaics.

2. Results and Discussion

2.1. Synthesis and characterization of copolymer additives.

Nine copolymers were targeted each with a different sequence and/or composition. The copolymers had a poly(3-hexylthiophene) backbone with varying quantities and distributions of side-chain fullerenes. Catalyst-transfer polymerization (CTP)[16] was used to access all copolymers with random, gradient, and block sequences, narrow dispersities (Đ), and high regioregularities (Scheme 1). Polymers with approximately the same number-average molecular weights (M_n) were targeted by using the same monomer/catalyst ratio for each polymerization. Using a precatalyst with an *ortho*-tolyl reactive ligand[15, 17, 18] ensured unidirectional propagation and led to polymers with tolyl/H end-groups. Activated (5-bromo-4-hexylthiophen-2-yl)magnesium chloride (HT) and (5-bromo-4-(6-bromohexyl)thiophen-2-yl)magnesium chloride (BrHT) were chosen as monomers to generate polymers with specified reactive side-chain distributions. Using this approach, we synthesized random, gradient, and diblock[19] copolymers with three different theoretical HT:BrHT ratios (80:20, 65:35, and 50:50, Supporting Information, SI pgs S23–S43.)[15]

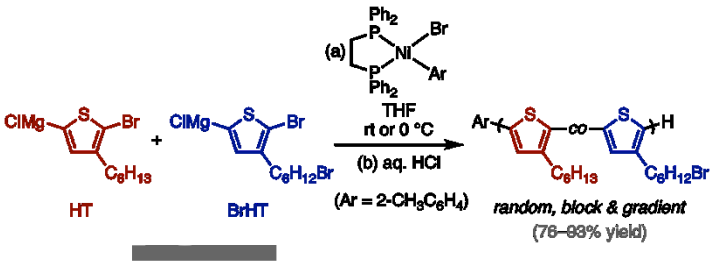

Scheme 1. Copolymer synthesis with random, block, and gradient distributions of Br-functionalized side chains.

The gradient copolymers were prepared by initiating HT polymerization and then gradually adding BrHT. The block copolymers were prepared by adding precatalyst to a solution containing HT; once the HT consumption reached >90%, BrHT was added. The random copolymers were prepared by adding precatalyst to a solution containing both HT and BrHT. A random (rather than statistical) sequence was obtained due to the similar monomer reactivities.[14e] The cumulative mole fraction incorporation of BrHT (f_{BrHT}) versus the copolymer's normalized chain length was evaluated by running an independent set of polymerizations where aliquots were periodically removed (Figure 1). As anticipated, the random copolymer showed a consistent, cumulative HT:BrHT ratio, whereas the block and gradient copolymers showed a changing HT:BrHT ratio consistent with the time-dependent changes in relative monomer concentrations during the reaction.

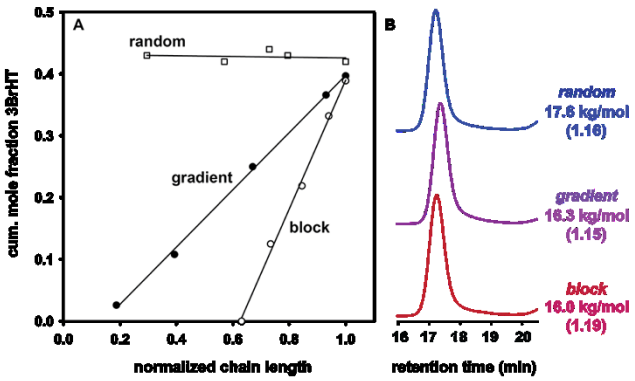

Figure 1. (A) Plot of the cumulative BrHT mole fraction in each copolymer versus its normalized chain length with a total monomer feed ratio of 60:40 HT:BrHT.[20] (B) GPC traces for the polymers obtained at normalized chain length = 1 (M_n and Đ are shown).

For each copolymer, a chain length of 80 thiophene units was targeted using a monomer/catalyst ratio of 80/1, which would give theoretical M_n of ~14–15 kg/mol depending on the BrHT mole fraction. The experimental M_n ranged from 18–22 kg/mol, consistent with the known overestimation of GPC by a factor of ~1.3x when using polystyrene calibration standards (Table 1).[21] As anticipated for CTP, each copolymer sample exhibited low dispersity (Đ = 1.11–1.24) and high regioregularity (SI pgs S35–S44). In addition, the mole fraction of BrHT incorporated into the copolymer (f_{BrHT}) matched the experimental feed ratios, implying that their conversion rates were similar.

Table 1. Data for Copolymers with Br-functionalized Side Chains.

	block			random			gradient		
BrHT:H	50:50	35:65	20:80	50:50	35:65	20:80	50:50	35:65	20:80

T (mol:mol)									
M_n (kg/mol)	18.8	19.1	19.5	21.1	21.4	21.7	20.7	22.1	18.9
Đ	1.19	1.17	1.15	1.24	1.23	1.22	1.15	1.11	1.19
f_{BrHT}	0.52	0.36	0.21	0.51	0.35	0.21	0.53	0.34	0.20

Two post-polymerization reactions were used to append fullerene units onto the copolymer side chains. The first reaction used sodium azide to substitute the side-chain bromine with an azide, generating a reactive handle for the click reaction (Scheme 2).[15,22] Subsequent ^{1}H NMR spectroscopic analysis revealed quantitative conversion of the Br to N_3. In addition, there were no significant changes in the GPC profiles. The second reaction involved an azide–alkyne 'click' reaction to install the fullerene moieties onto the side chain. In our previous work, we used the copper-catalyzed azide–alkyne cycloaddition;[15a] however, crosslinked polymers were obtained when the azide concentration exceeded 10 mol%. To prevent this deleterious side-reaction, we employed the strain-promoted azide–alkyne cycloaddition (SPAAC) that proceeds without a copper catalyst.[23] This approach involved 5 linear steps to synthesize the strained alkyne fullerene derivative, with a 14% overall yield from commercial starting materials (Scheme 3, SI pgs S8–S11). Although low yielding, most alternative methods for grafting fullerene to P3HT require harsher conditions, including [3+2] cycloadditions,[12f,12h,24] 1,3-dipolar cycloadditions,[12a,25] and S_N2 reactions.[26] In contrast, the Steglich esterification[27] and

Diels-Alder cycloaddition[28] represent mild alternatives to SPAAC for grafting fullerenes to P3HT. Our route began with ring-expansion of dibenzosuberenone followed by reduction with sodium borohydride.[29] Subsequent dibromination followed by a double elimination with lithium diisopropylamide afforded dibenzocyclooctynol (DIBO) in moderate yield.[29] In a separate step, the methyl ester of $PC_{61}BM$ was converted to the corresponding acid via hydrolysis.[30] Esterifying this acid with DIBO in the presence of *N,N'*-diisopropylcarbodiimide yielded the click-ready fullerene derivative $PC_{61}B$-DIBO.[15]

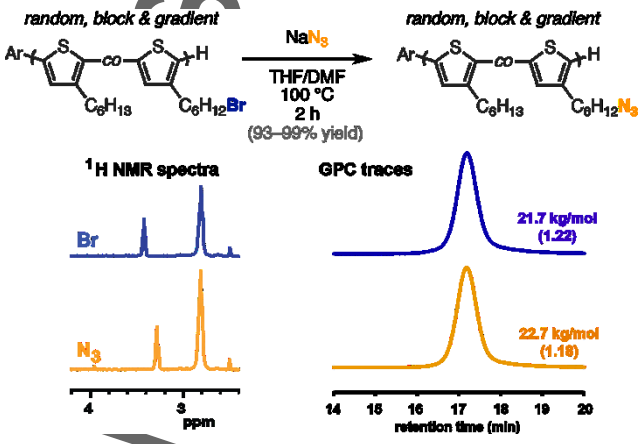

Scheme 2. Post-polymerization reaction to generate random, block and gradient copolymers with N_3-functionalized side chains. ^{1}H NMR spectra and GPC traces of the random copolymer (20 mol%) before and after the reaction.

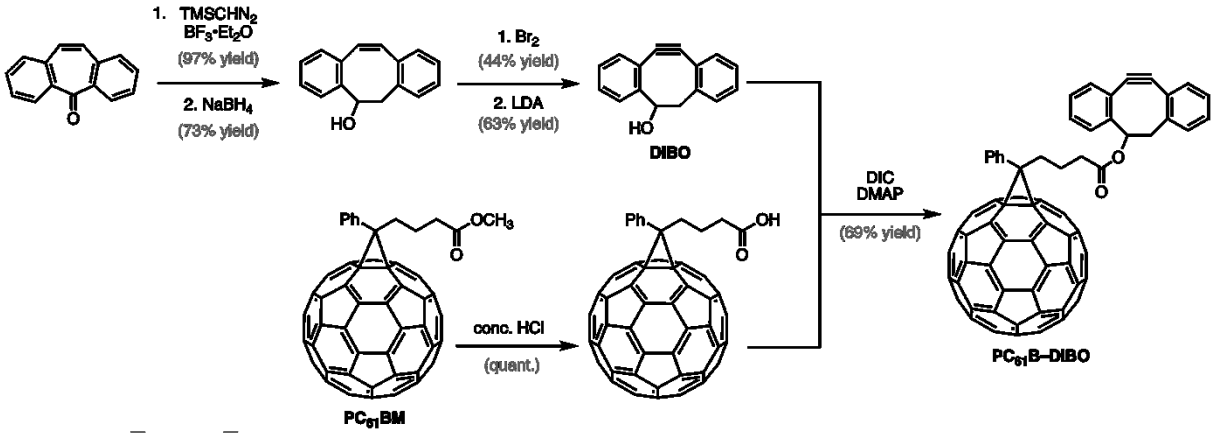

Scheme 3. Synthetic route to generate $PC_{61}B$-DIBO from dibenzosuberenone and $PC_{61}BM$.

Each of the nine copolymers were functionalized with fullerene via SPAAC by stirring the azide-functionalized copolymer with $PC_{61}BM$-DIBO at room temperature over 48 h (Scheme 4, SI pgs S51–S56).[31,32] The fullerene-loaded copolymers were characterized using IR spectroscopy to confirm >95% azide conversion via disappearance of the peak at 2091 cm^{-1}.[33] Comparing the copolymers to a fullerene-functionalized small-molecule analog (SI pgs S22–S23) via ^1H NMR spectroscopy supported cycloadduct formation. Multiple stereo- and regioisomers were generated due to both the racemic **$PC_{61}B$-DIBO** and the non-regioselective reaction. Combined, these results indicate that fullerene-functionalized copolymers with varying sequences and compositions were obtained.

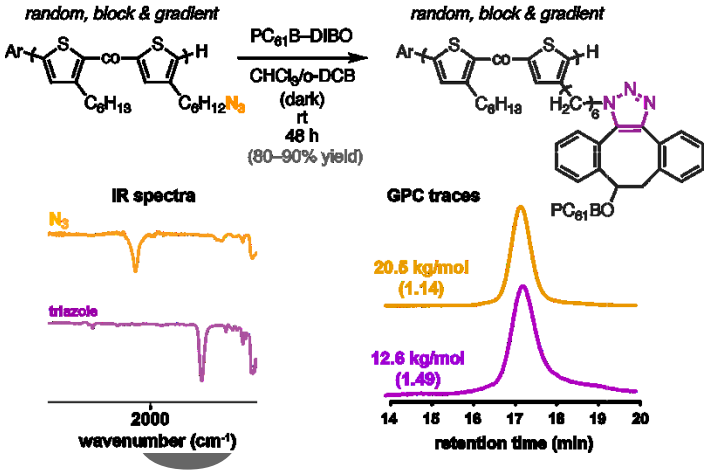

Scheme 4. Post-polymerization transformation to generate random, block and gradient copolymers with fullerene-functionalized side chains. IR spectra and GPC traces of the block copolymer (20 mol%) before and after the reaction.

2.2 Quantifying Phase Separation in Blends

As noted above, one of the biggest challenges for polymer-based photovoltaics is their unstable active layer morphologies,[7] which form micron-scale domains with reduced interfacial area over time. We hypothesized that fullerene-functionalized P3HT copolymers could enthalpically stabilize P3HT:$PC_{61}BM$ blends, minimizing their micron-scale phase separation. To test this hypothesis, we examined the thermal stability of P3HT:$PC_{61}BM$ blends with and without each copolymer additive using optical microscopy.

The benchmark was set by annealing P3HT:$PC_{61}BM$ (1:1 wt:wt) blends for 1 h at 150 °C. Subsequent optical microscope images revealed needle-shaped $PC_{61}BM$ aggregates[34] (~5–30 mm length and ~1 mm width) occupying 11.4% of the film area (Figure 2A). Next, blends with different copolymer sequences and compositions were co-deposited with P3HT:$PC_{61}BM$ at several different concentrations. After thermal annealing, optical microscope images revealed

that all copolymer additives led to reduced sizes and densities of $PC_{61}BM$ aggregates (Figure 2B–D, SI pgs S57–S59).

Plotting these data as a function of the copolymer variables revealed that the random and gradient sequences outperformed the diblock sequence regardless of the composition or concentration (Figure 2E). We suspect that this effect is entropic in origin, wherein the gradient and random copolymers have more low-energy orientations at the interface (than the block) due to their mixed composition. When comparing copolymers of the same sequence and composition but at different concentrations in the blend (e.g., 2 versus 8 wt%), we found that higher copolymer concentrations were better, presumably because more of the interfacial area can be stabilized under these conditions. When comparing copolymers with the same sequences but different compositions (e.g., random 50 versus 20 mol%), the higher fullerene loading exhibited *more* phase separation. In this case, less compatibilizer is added to the blend when the fullerene-loading is higher because the average 'repeat unit' mass is higher; consequently, less interfacial area is stabilized under these conditions. In total, these data suggested that the most stable devices would be obtained with random and/or gradient copolymers at 20 mol% fullerene loading and at 8 wt% concentration in the blend.

These conclusions are further supported by UV/vis spectroscopic data collected on selected films before and after thermal annealing (SI Figure S55). The blend with no additive showed substantial phase separation after annealing as evidenced by a drop in the $PC_{61}BM$ signal (due to crystallization) and an increase in the P3HT peak intensity (due to de-mixing). In contrast, a blend containing random copolymer (20 mol% fullerene, at 8 wt% concentration) showed no change in the $PC_{61}BM$ intensity and only a small increase in P3HT intensity after thermal annealing.

Combined, these results indicate that all copolymers suppress phase separation in P3HT:$PC_{61}BM$ blends, presumably by serving as an interfacial compatibilizer. One alternative explanation is that the copolymer increases the glass transition temperature of the blend (T_g^{blend}), which would minimize phase separation at the temperatures studied herein. To evaluate this hypothesis, the T_g^{blend} was measured for blends with and without added copolymer via differential scanning calorimetry (DSC). Blends without the copolymers exhibited a weak, broad T_g^{blend} at 42 °C, consistent with previous reports (SI Figure S69).[35] In contrast, blends containing the copolymer additive did not exhibit a discernable T_g^{blend}, regardless of sample mass, scan rate, scan range, and even with a modulated temperature profile (SI pgs S69–71). At this time, the precise mechanism for the stabilization remains unclear.

Among the 28 films examined, the random and gradient copolymers showed the least macroscale phase separation overall. Because the random copolymer with 20 mol% fullerene side chains and at 8 wt% concentration was both the best compatibilizer and the easiest to access synthetically, we focused the following device studies on this copolymer alone, comparing P3HT:$PC_{61}BM$ blends with and without it.

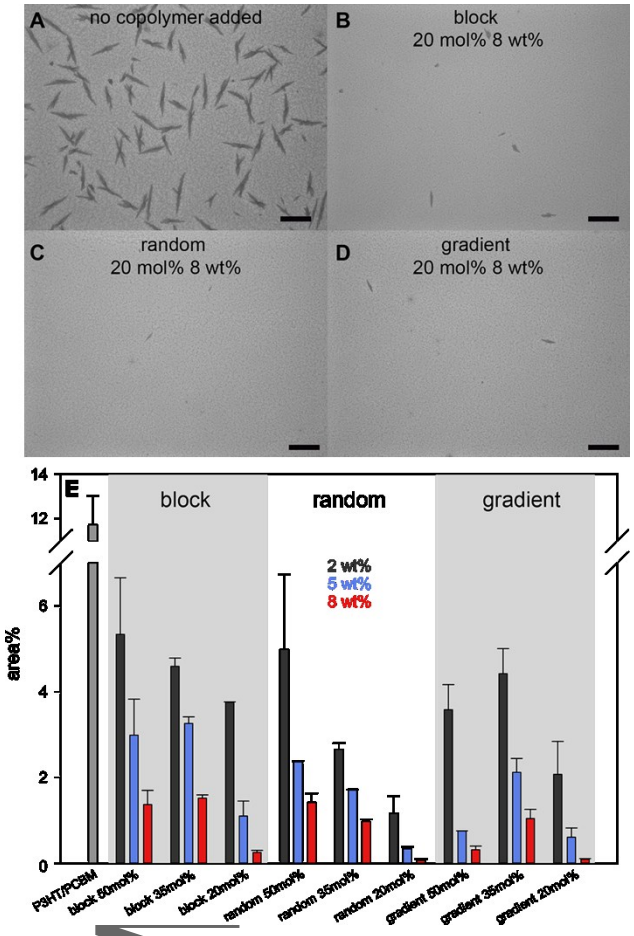

Figure 2. (A–D) Optical microscope images of P3HT:copolymer additive:$PC_{61}BM$ blends after annealing at 150 °C for 1 h (scale bar = 30 μm). (E) The relative area% of $PC_{61}BM$ aggregates within each blend as a function of the copolymer sequence, composition and concentration.

2.3 Device Performance and Longevity

The PCE depends on the efficiencies of absorption and exciton dissociation, as well as the electron and hole mobilities. Although we anticipated that the random copolymer devices would have a more stable PCE during annealing due to the copolymer's morphology-stabilizing properties, it was unclear what effect the copolymer additive would have on the other processes

that contribute to PCE. To elucidate its effect, photovoltaic devices were fabricated using an inverted device architecture: glass/ITO/ZnO/polymer blend/MoO_3/Ag (SI pg S5).[36] The polymer blend was prepared by spin-casting a P3HT:$PC_{61}BM$ solution with or without random copolymer additive to achieve a final thickness of ~175 nm (SI pgs S3–S4). Photovoltaic measurements were performed under simulated AM 1.5G conditions both before and after annealing. To obtain statistically significant results, each data point represents an average of six measurements obtained from three different devices fabricated on two different substrates.

Devices containing the random copolymer additive exhibited an unexpectedly higher initial PCE (3.1 ± 0.2%) than the control device (2.4 ± 0.2%) (Figure 3A, SI Figures S56 and S57). The observed PCE increase is largely attributable to a higher fill factor (FF), which is proportional to the maximum power available from a solar cell (Figure 3B). This FF difference is not due to an increase in the absorption efficiency because the copolymer has a nearly identical absorption spectrum to the P3HT:$PC_{61}BM$ blend (SI Figure S62). We hypothesized that the copolymer might instead facilitate exciton dissociation because its HOMO and LUMO levels both lie between those of P3HT and $PC_{61}BM$, providing an 'energy cascade' (Figure 3C, SI Figures S62 and S63).[37] In addition, we observed that the electron current was significantly higher in the blends containing the random copolymer than those with none (202 ± 47 pA/μm^2 versus 88 ± 11 pA/μm^2, SI Figure S64).[38] This increased electron mobility may be due to better charge migration away from the interface through the fullerene units in the copolymer (Scheme 5). To support this hypothesis, we compared the series resistances (R_s), which reflects the overall device resistance (Figure 3D). The device containing random copolymer exhibited a significantly lower series resistance, consistent with the notion that the copolymer plays an active role in exciton dissociation and electron percolation. Last, atomic force microscope

images revealed that the films containing random copolymer exhibited smaller feature sizes with larger interfacial area than the control (SI Figure S65). More interfacial area should translate to more efficient excitons dissociation, and an ensuing higher PCE. To summarize these studies, the random copolymer had an unanticipated beneficial impact on the initial device PCE by enhancing both exciton dissociation and electron percolation and mobility.

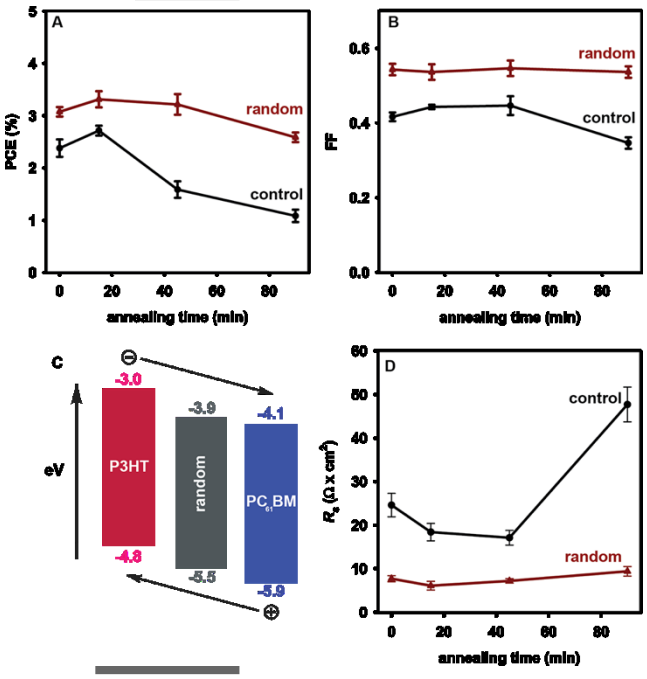

Figure 3. Plots of the (A) power conversion efficiency (PCE), (B) fill factor (FF), and (D) series resistance (R_s) versus annealing time for P3HT:$PC_{61}BM$ devices with and without random copolymer. (C) Schematic comparing the HOMO/LUMO levels of the copolymer relative to P3HT and $PC_{61}BM$.

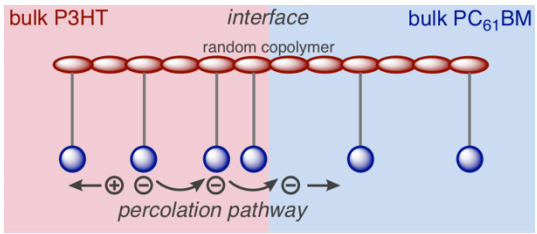

Scheme 5. Proposed percolation pathway in which electron mobility is facilitated at the interface by the side chain fullerenes on the random copolymer.

To determine device stabilities over time, thermal studies were performed by annealing the active layer at 150 °C before MoO_3/Ag deposition. Devices containing random copolymer significantly outlasted and outperformed the control devices (Figure 3 and SI pgs 60–63). After annealing for 90 min the control device lost >50% of its initial PCE; however, the random copolymer-containing device lost just 15% of its initial PCE (Figure 3A). The biggest change in the control device was a significant drop (>50%) in the short-circuit current (J_{sc}), which reflects charge generation and collection processes (SI Figure S57). This result can be rationalized in conjunction with the micron-scale phase segregation occurring during this time. These morphological changes reduce the donor/acceptor interfacial area, decreasing the exciton dissociation efficiency. This conclusion is supported by the changes in *Rs*,[39] which for the control device increases from 24.6 to 47.7 Ω×cm^2 after annealing (Figure 3D). Combined, these data suggest that by stabilizing the active layer morphology, the random copolymer compatibilizer also stabilizes the device PCE.

Although the random copolymer led to a longer-lasting device, a minor but significant drop in PCE was observed. The culprit was a decrease in open-circuit voltage (V_{oc}, SI Figure S57), which reflects the amount of charge recombination. Further analysis showed that the reverse bias saturation current (J_0),[40] which also reflects the amount of charge recombination, was one order of magnitude higher with random copolymer present (SI Figure S61). The theoretical V_{oc} changes expected from this J_0 difference is ~ 0.07 *V,* consistent with the experimental differences in V_{oc} (SI pg S65). Combined, the V_{oc} drop and increased J_0 implies that after annealing the copolymer additive facilitates some charge recombination.

3. Conclusions

While PCEs have been on the rise for organic photovoltaics, the poor longevity of these devices remains a concern. We demonstrated that a random copolymer additive can both enhance longevity and improve efficiency. Other areas for future exploration include understanding the increased charge recombination that occurs after annealing as well as how the transport layer interfaces are affected by compatibilizer. Overall, this approach to stabilizing organic photovoltaics should be generalizable, and our future efforts are focused on applying it toward higher efficiency conjugated polymer-based devices.

Supporting Information

Supporting Information is available from the Wiley Online Library.

Acknowledgements

We thank J. Wenderoff for assistance with AFM analysis. AJM gratefully acknowledges the Army Research Office (ARO Grant 58200-CH-PCS) for support of this work. JK gratefully acknowledges the Qatar National Research Fund (NPRP8-245-1-059) for partial support this work.

Received: ((will be filled in by the editorial staff))
Revised: ((will be filled in by the editorial staff))
Published online: ((will be filled in by the editorial staff))

Photovoltaic devices made from conjugated polymers now exhibit efficiencies rivaling amorphous silicon; however, the poor longevity of these devices continues to stymie their commercial impact. Copolymer additives represent a promising solution, yet little is known about how the copolymer sequence, composition and concentration influence their compatibilizing abilities in the blend. Herein, random copolymer additives led to higher efficiency and longer-lasting photovoltaic devices.

Keywords: conjugated polymers, fullerenes, polymer blends, organic photovoltaics

Chen Kong, Byeongseop Song, Emily A. Mueller, Jinsang Kim and Anne J. McNeil

Random Copolymers Outperform Gradient and Block Copolymers in Stabilizing Organic Photovoltaics.

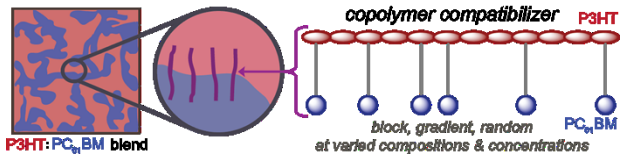

(1) National Renewable Energy Lab, Best Research-cell Efficiencies, https://www.nrel.gov/pv/assets/images/efficiency-chart.png, accessed: June 2018

(2) For recent reviews, see: (a) G. Zhang, J. Zhao, P. C. Y. Chow, K. Jiang, J. Zhang, Z. Zhu, J. Zhang, F. Huang, H. Yan, *Chem. Rev.* **2018**, *118*, 3447–3507. (b) J. Hou, O. Inganäs, R. H. Friend, F. Gao, *Nature Mater.* **2018**, *17*, 119–128. (c) S. Holliday, Y. Li, C. K. Luscombe, *Prog. Polym. Sci.* **2017**, *70*, 34–51. (d) H. Huang, L. Yang, B. Sharma, *J. Mater. Chem. A* **2017**, *5*, 11501–11517. (e) Y. Gao, M. Liu, Y. Zhang, Z. Liu, Y. Yang, L. Zhao, *Polymers* **2017**, *9*, 39. (f) Z. Hu, L. Ying, F. Huang, Y. Cao, *Sci. China Chem.* **2017**, *60*, 571–582. (g) S. Xiao, Q. Zhang, W. You, *Adv. Mater.* **2017**, *29*, 1601391. (h) L. Ying, F. Huang, G. C. Bazan, *Nature Commun.* **2017**, *8*, 14047.

(3) (a) F. C. Krebs, N. Espinosa, M. Hösel, R. R. Søndergaard, M. Jørgensen, *Adv. Mater.* **2014**, *26*, 29–39. (b) R. R. Søndergaard, M. Hösel, F. C. Krebs, *J. Polym. Sci. Part B: Polym. Phys.* **2013**, *51*, 16–34. (c) R. Søndergaard, M. Hösel, D. Angmo, T. T. Larsen-Olsen, F. C. Krebs, *Mater. Today* **2012**, *15*, 36–49.

(4) For reviews and recent examples of fullerene-free devices, see: (a) G. Zhang, J. Zhao, P. C. Y. Chow, K. Jiang, J. Zhang, Z. Zhu, J. Zhang, F. Huang, H. Yan, *Chem. Rev.* **2018**, 118, 3447–3507. (b) S. Li, L. Ye, W. Zhao, H. Yan, B. Yang, D. Liu, W. Li, H. Ade, J. Hou, *J. Am. Chem. Soc.* **2018**, *140*, 7159–7167. (c) Z. Fei, F. D. Eisner, X. Jiao, M. Azzouzi, J. A. Röhr, Y. Han, M. Shahid, A. S. R. Chesman, C. D. Easton, C. R. McNeill, T. D. Anthopoulos, J. Nelson, M. Heeney, *Adv. Mater.* **2018**, *30*, 1705209. (d) P. Cheng, G. Li, X. Zhan, Y. Yang, *Nature Photonics* **2018**, *12*, 131–142. (e) X. Xu, T. Yu, Z. Bi, W. Ma, Y. Li, Q. Peng, *Adv. Mater*. **2018**, *30*, 1703973. (f) W. Zhao, S. Li, H. Yao, S. Zhang, Y. Zhang, B. Yang, J. Hou, *J. Am. Chem. Soc.* **2017**, *139*, 7148–7151. (g) W. Chen, Q. Zhang, *J. Mater. Chem. C* **2017**, *5*, 1275–1302.

(5) For reviews and examples of fullerene-containing devices, see: (a) J. Zhao, S. Zhao, Z. Xu, D. Song, B. Qiao, D. Huang, Y. Zhu, Y. Li, Z. Li, Z. Qin, *ACS Appl. Mater. Interfaces* DOI: 10.1021/acsami.8b07342. (b) C. Xu, M. Wright, N. K. Elumalai, M. A. Mahmud, D. Wang, V. R. Goncales, M. B. Upama, F. Haque, J. J. Gooding, A. Uddin. *Appl. Phys. A* **2018**, *124*, 449. (c) Y. Liu, M. Sheri, M. D. Cole, T. Emrick, T. P. Russell, *Angew. Chem. Int. Ed*. **2018**, *57*, DOI: 10.1002/anie.201803748. (d) J. Zhang, R. Xue, G. Xu, W. Chen, G.-Q. Bian, C. Wei, Y. Li, Y. Li, *Adv. Funct. Mater.* **2018**, *28*, 1705847. (e) X. Liu, L. Nian, K. Gao, L. Zhang, L. Qing, Z. Wang, L. Ying, Z. Xie, Y. Ma, Y. Cao, F. Liu, J. Chen. *J. Mater. Chem. A* **2017**, *5*, 17619–17631. (f) C. Li, H. Zhu, Y.

Wang, H. Liu, S. Hu, F. Wang, B. Zhang, S. Dai, Z. Tan, *Nano Energy* **2017**, *31*, 201–209. (g) J. Huang, J. H. Carpenter, C.-Z. Li, J.-S. Yu, H. Ade, A. K.-Y. Jen, *Adv. Mater.* **2016**, *28*, 967–974. (h) J. Zhao, Y. Li, G. Yang, K. Jiang, H. Lin, H. Ade, W. Ma, H. Yan, *Nat. Energy* **2016**, *1*, 15027.

(6) K. Bourzac, *C&EN Global Enterp*. **2018**, *96 (22)*, 7–7.

(7) For reviews on stability (including, but not limited to, morphological stability), see: (a) S. Rafique, S. M. Abdullah, K. Sulaiman, M. Iwamoto, *Renew. Sust. Energy Rev.* **2018**, *84*, 43–53. (b) S. A. Gevorgyan, I. M. Heckler, E. Bundgaard, M. Corazza, M. Hösel, R. R. Søndergaard, G. A. dos Reis Benatto, M. Jørgensen, F. C. Krebs, *J. Phys. D: Appl. Phys.* **2017**, *50*, 103001. (c) W. R. Mateker, M. D. McGehee, *Adv. Mater.* **2017**, *29*, 1603940. (d) P. Cheng, X. Zhan, *Chem. Soc. Rev.* **2016**, *45*, 2544–2582. (e) S. Lizin, S. Van Passel, E. De Schepper, W. Maes, L. Lutsen, J. Manca, D. Vanderzande, *Energy Environ. Sci.* **2013**, *6*, 3136–3149. (f) M. Jørgensen, K. Norrman, S. A. Gevorgyan, T. Tromholt, B. Andreasen, F. C. Krebs, *Adv. Mater.* **2012**, *24*, 580–612.

(8) (a) B. Kuei, E. D. Gomez, *Soft Matter* **2017**, *13*, 49–67. (b) F. S. Bates, *Science* **1991**, *251*, 898–905.

(9) For recent reviews, see: (a) P. Cheng, X. Zhan, *Mater. Horiz.* **2015**, *2*, 462–485. (b) Goubard, G. Wantz, *Polym. Int.* **2014**, *63*, 1362–1367.

(10) For recent examples, see: (a) M. Xiao, K. Zhang, Y. Jin, Q. Yin, W. Zhong, F. Huang, Y. Cao, *Nano Energy* **2018**, *48*, 53–62. (b) G. Sai-Anand, A. Dubey, A.-I. Gopalan, S. Venkatesan, S. Ruban, K. M. Reza, J. Choi, K. S. Lakhi, B. Xu, Q. Qiao, A. Vinu, *Sol. Energy Materials and Sol. Cells* **2018**, *182*, 246–254. (c) A. Rahmanudin, X. A. Jeanbourquin, S. Hänni, A. Sekar, E. Ripaud, L. Yaoa, K.

Sivula, *J. Mater. Chem. A* **2017**, *5*, 17517–17524. (d) H. Li, K. Lu, Z. Wei, *Adv. Energy Mater.* **2017**, *7*, 1602540. (d) P. Cheng, C. Yan, T-K. Lau, J. Mai, X. Lu, X. Zhan, *Adv. Mater.* **2016**, *28*, 5822–5829. (e) P. Cheng, Q. Shi and X. Zhan, *Acta Chim. Sin.* **2015**, *73*, 252–256. (f) W. Zhou, J. Shi, L. Lv, L. Chen and Y. Chen, *Phys. Chem. Chem. Phys.* **2015**, *17*, 387–397. (g) J. Yang, W. He, K. Denman, Y. Jiang and Y. Qin, *J. Mater. Chem. A* **2015**, *3*, 2108–2119. (h) Q. An, F. Zhang, L. Li, J. Wang, Q. Sun, J. Zhang, W. Tang and Z. Deng, *ACS Appl. Mater. Interfaces* **2015**, 7, 3691–3698. (i) W. Nie, G. Gupta, B. K. Crone, F. Liu, D. L. Smith, P. P. Ruden, C.-Y. Kuo, H. Tsai, H.-L. Wang, H. Li, S. Tretiak and A. D. Mohite, *Adv. Sci.* **2015**, *2*, 1500024. (j) S. Wang, Y. Qu, S. Li, F. Ye, Z. Chen, X. Yang, *Adv. Funct. Mater.* **2015**, *25*, 748–757.

(11) For recent reviews, see: (a) D. Kipp, R. Verduzco, V. Ganesan, *Mol. Syst. Des. Eng.* **2016**, *1*, 353–369. (b) K. Yuan, L. Chen, Y. Chen, *Polym. Int.* **2014**, *63*, 593–606. (c) See also, ref 9a.

(12) For recent examples, see: (a) C. Sartorio, V. Campisciano, C. Chiappara, S. Cataldo, M. Scopelliti, M. Gruttadauria, F. Giacalone, B. Pignataro, *J. Mater. Chem. A* **2018**, *6*, 3884–3498. (b) Y. Sun, P. Pitliya, C. Liu, X. Gong, D. Raghavan, A. Karim, *Polymer* **2017**, *113*, 135–146. (c) D. Kipp, O. Wodo, B. Ganapathysubramanian, V. Ganesan, *Sol. Energy Mater. Sol. Cell* **2017**, *161*, 206–218. (d) F. Lombeck, A. Sepe, R. Thomann, R. H. Friend, M. Sommer, *ACS Nano* **2016**, *10*, 8087–8096. (e) H. Fujita, T. Michinobu, S. Fukuta, T. Koganezawa, T. Higashihara, *ACS Appl. Mater. Interfaces* **2016**, *8*, 5484–5492. (f) S. Kakogianni, A. K. Andreopoulou, J. K. Kallitsis, *Polymers* **2016**, *8*, 440. (g) D. Kipp, V. Ganesan, *Macromolecules* **2016**, *49*, 5137–5144. (h) S. Kakogianni, M. A. Lebedeva, G. Paloumbis, A. K. Andreopoulou, K. Porfyrakis, J. K. Kallitsis, *RSC Adv.* **2016**, *6*, 98306–98316. (i) J. W. Mok, D. Kipp, L. R. Hasbun, A. Dolocan, J. Strzalka, V. Ganesan, R. Verduzco, *J. Mater.*

Chem. A **2016**, *4*, 14804–14813. (j) J. Liu, X. Zhu, J. Li, J. Shen, G. Tu, *RSC Adv.* **2016**, *6*, 61934–61943. (k) K. H. Park, Y. An, S. Jung, H. Park, C. Yang, *Energy Environ. Sci.* **2016**, *9*, 3464–3471. (l) E. Bicciocchi, M. Haeussler, E. Rizzardo, A. D. Scully, K. P. Ghiggino, *J. Polym. Sci., Part A: Polym. Chem.* **2015**, *53*, 888–903. (m) M. Raïssi, H. Erothu, E. Ibarboure, H. Cramail, L. Vignau, E. Cloutet, R. C. Hiorns *J. Mater. Chem. A* **2015**, *3*, 18207–18221. (m) D. Kipp, J. Mok, J. Strzalka, S. B. Darling, V. Ganesan, R. Verduzco, *ACS Macro Lett.* **2015**, *4*, 867–871.

(13) A. Li, J. Amonoo, B. Huang, P. K. Goldberg, A. J. McNeil, P. F. Green, *Adv. Funct. Mater.* **2014**, *24*, 5594–5602.

(14) (a) J. A. Amonoo, A. Li, G. E. Purdum, M. E. Sykes, B. Huang, E. F. Palermo, A. J. McNeil, M. Shtein, Y.-L. Loo, P. F. Green, *J. Mater. Chem. A* **2015**, *3*, 20174–20184. (b) E. F. Palermo, A. J. McNeil, In *Sequence-Controlled Polymers: Synthesis, Self-Assembly, and Properties*, (Eds: H. Baltes, W. Göpel, J. Hesse), ACS Symposium Series, American Chemical Society, Washington, DC **2014**, Ch. 19. (c) E. F. Palermo, H. L. van der Laan, A. J. McNeil, *Polym. Chem.* **2013**, *4*, 4606–4611. (d) E. F. Palermo, A. J. McNeil, *Macromolecules* **2012**, *45*, 5948–5955. (e) J. R. Locke, A. J. McNeil, *Macromolecules* **2010**, *43*, 8709–8710.

(15) E. F. Palermo, S. B. Darling, A. J. McNeil, *J. Mater. Chem. C* **2014**, *2*, 3401–3406.

(16) For recent reviews, see: (a) M. A. Baker, C.-H. Tsai, K. J. T. Noonan, *Chem. Eur. J.* **2018**, *24*, DOI: 10.1002/chem.201706102. (b) A. K. Leone, A. J. McNeil, *Acc. Chem. Res.* **2016**, *49*, 2822–2831. (c) T. Yokozawa, Y. Ohta, *Chem. Rev.* **2016**, *116*, 1950–1968. (d) R. Grisorio, G. P. Suranna,

Polym. Chem. **2015**, *6*, 7781–7795. (e) Z. J. Bryan, A. J. McNeil, *Macromolecules* **2013**, *46*, 8395–8405.

(17) (a) H. A. Brontstein, C. K. Luscombe, *J. Am. Chem. Soc.* **2009**, *131*, 12894–12895. (b) N. Doubina, A. Ho, A. K.-Y. Jen, C. K. Luscombe, *Macromolecules* **2009**, *42*, 7670–7677. (c) V. Senkovskyy, R. Tkachov, T. Beryozkina, H. Komber, U. Oertel, M. Horecha, V. Bocharova, M. Stamm, S. A. Gevorgyan, F. C. Krebs, A. Kiriy, *J. Am. Chem. Soc.* **2009**, *131*, 16445–16453. (d) V. Senkovskyy, M. Sommer, R. Tkachov, H. Komber, W. T. S. Huck, A. Kiriy, *Macromolecules* **2010,** *43*, 10157–10161.

(18) See also: (a) A. O. Hall, S. R. Lee, A. N. Bootsma, J. W. G. Bloom, S. E. Wheeler, A. J. McNeil, *J. Polym. Sci., Part A: Polym. Chem.* **2017**, *55*, 1530–1535. (b) S. R. Lee, J. W. G. Bloom, S. E. Wheeler, A. J. McNeil, *Dalton Trans.* **2013**, *42*, 4218–4222. (c) E. L. Lanni, A. J. McNeil, *J. Am. Chem. Soc.* **2009**, *131*, 16573–16579.

(19) For a related structure, see: S. H. Chan, C. S. Lai, H. L. Chen, C. Ting, C. P. Chen, *Macromolecules* **2011**, *44*, 8886–8891.

(20) All copolymerizations presented in Figure 1 were conducted under N_2 (outside the glovebox) at 0 °C so that the slower reaction rate would enable adequate time between aliquots.

(21) M. Wong, J. Hollinger, L. M. Kozycz, T. M. McCormick, Y. Lu, D. C. Burns, D. S. Seferos, *ACS Macro Lett.* **2012**, *1*, 1266–1269.

(22) See also: L. Zhai, R. L. Pilston, K. L. Zaiger, K. K. Stokes, R. D. McCullough, *Macromolecules* **2003**, *36*, 61–64.

(23) For a recent review, see: C. J. Pickens, S. N. Johnson, M. M. Pressnall, M. A. Leon, C. J. Berkland, *Bioconjugate Chem.* **2018**, *29*, 686–701.

(24) S.-H. Chan, C.-S. Lai, H.-L. Chen, C. Ting, C.-P. Chen, *Macromolecules* **2011**, *44*, 8886–8891.

(25) M. Li, P. Xu, J. Yang, S. Yang, *J. Mater. Chem.* **2010**, *20*, 3953–3960.

(26) (a) F. Pierini, M. Lanzi, P. Nakielski, S. Pawlowska, O. Urbanek, K. Zembrzcyki, T. A. Kowalewski, *Macromolecules* **2017**, *50* 13, 4972–4981. (b) M. Lanzi, E. Salatelli, T. Benelli, D. Caretti, L. Giorgini, F. P. Di-Nicola, *J. Appl. Polym. Sci.* **2015**, *132*, 42121.

(27) M. Chen, M. Li, H. Wang, S. Qu, X. Zhao, L. Xie, S. Yang, *Polym. Chem.* **2013**, *4*, 550–557.

(28) B. Yameen, T. Puerchkhauer, J. Ludwig, I. Ahmed, O. Altintas, L. Fruk, A. Colsmann, C. Barner-Kowollik, *Small* **2014**, *10*, 3091–3098.

(29) N. E. Mbua, J. Guo, M. A. Wolfert, R. Steet, G.-J. Boons *ChemBioChem* **2011**, *12*, 1912–1921.

(30) S. P. Singh, CH. P. Kumar, G. D. Sharma, R. Kurchania, M. S. Roy, *Adv. Funct. Mater.* **2012**, *22*, 4087–4095.

(31) S. Wang, X. Yang, W. Zhu, L. Zou, K. Zhang, Y. Chen, F. Xi, *Polymer* **2014**, *55*, 4812–4819.

(32) Copolymers with >50 mol% side-chain fullerenes were largely insoluble in THF and not pursued further.

(33) An exothermic peak was observed at temperatures >150 °C during DSC analysis of some fullerene-functionalized copolymers (SI Figures S66–S67). After DSC analysis, the samples were completely insoluble in $CDCl_3$. We tentatively attributed this non-reversible event to a crosslinking reaction involving side-chain azides (<5% by IR spectroscopy) reacting with fullerene. Fortunately, this reaction does not occur if the copolymer samples are heated to the device annealing temperature (150 °C). After DSC analysis, the resulting copolymers fully dissolve in $CDCl_3$ and the ^1H NMR spectra are identical to the samples before analysis (SI Figure S67).

(34) A. Torreggiani, F. Tinti, A. Savoini, M. Melchiorre, R. Po, N. Camaioni, *Org. Photonics Photovolt.* **2014**, *2*, 50–58.

(35) (a) J. Zhao, A. Swinnen, G. Van Assche, J. Manca, D. Vanderzande, B. Van Mele, *J. Phys. Chem. B* **2009**, *113*, 1587–1591. (b) P. E. Hopkinson, P. A. Staniec, A. J. Pearson, A. D. F. Dunbar, T. Wang, A. J. Ryan, R. A. L. Jones, D. G. Lidzey, A. M. Donald, *Macromolecules* **2011**, *44*, 2908–2917. (a) H. Chen, J. Chen, W. Yin, X. Yu, M. Shao, K. Xiao, K. Hong, D. L. Pickel, W. M. Kochemba, S. M. Kilbey II, M. Dadmun, *J. Mater. Chem. A* **2013**, *1*, 5309–5319.

(36) Z. He, C. Zhong, S. Su, M. Xu, H. Wu, Y. Cao, *Nature Photonics* **2012**, *6*, 591–595.

(37) (a) J. Hou, Z. Tan, Y. Yan, Y. He, C. Yang, Y. Li, *J. Am. Chem. Soc.* **2006**, *128*, 4911–4916. (b) Y. He, G. Zhao, B. Peng, Y. Li, *Adv. Funct. Mater.* **2010**, *20*, 3383–3389.

(38) Note that blends containing 12 wt% random copolymer exhibited lower electron mobilities than the 8 wt% blend, and lower hole mobilities than the control devices, suggesting there is an

upper limit to additive concentration on its beneficial effects (SI Figures S56–S57). We suspect that at these higher concentrations the copolymer may disrupt the P3HT crystallization within its "pure" domain.

(39) M.-S. Kim, B.-G. Kim, J. Kim, *ACS Appl. Mater. Interfaces* **2009**, *1*, 1264–1269.

(40) (a) J. D. Zimmerman, X. Xiao, C. K. Renshaw, S. Wang, V. V. Diev, M. E. Thompson, S. R. Forrest, *Nano Lett.* **2012**, *12*, 4366–4371. (b) W. J. Potscavage, Jr., A. Sharma, B. Kippelen, *Acc. Chem. Res.* **2009**, *42*, 1758–1767. (c) C. G. Shuttle, A. Maurano, R. Hamilton, B. O'Regan, J. C. de Mello, J. R. Durrant, *Appl. Phys. Lett.* **2008**, *93*, 183501.